



PAPER

[View Article Online](#)
[View Journal](#) | [View Issue](#)Cite this: *J. Mater. Chem. B*, 2023,
11, 9467A CD326 monoclonal antibody modified core
cross-linked curcumin-polyphosphoester prodrug
for targeted delivery and cancer treatment†Haijiao Li,^a Mingzu Zhang,^a Jinlin He, ^a Jian Liu, ^b Xingwei Sun*^c and
Peihong Ni ^{*a}

Stimuli-responsive cross-linked micelles (SCMs) are ideal nanocarriers for anti-cancer drugs. Compared with non-cross-linked micelles, SCMs exhibit superior structural stability. At the same time, the introduction of an environmentally sensitive crosslinker into a drug delivery system allows SCMs to respond to single or multiple stimuli in the tumor microenvironment, which can minimize drug leakage during the blood circulation process. In this study, curcumin (CUR) was modified as the hydrophobic core crosslinker by utilizing the bisphenol structure, and redox sensitive disulfide bonds were introduced to prepare the glutathione (GSH) stimulated responsive core crosslinker (abbreviated as N₃-ss-CUR-ss-N₃). In addition, amphiphilic polymer APEG-*b*-PBYP was prepared through the ring opening reaction, and reacted with the crosslinker through the “click” reaction. After being dispersed in the aqueous phase, core cross-linked nanoparticles (CCL NPs) were obtained. Finally, monoclonal antibody CD326 (mAb-CD326) was reduced and coupled to the hydrophilic chain ends to obtain the nanoparticles with surface modified antibodies (R-mAb-CD326@CCL NPs) for further enhancing targeted drug delivery. The structures of the polymer and crosslinker were characterized by ¹H NMR, UV-Vis, FT-IR, and GPC. The morphology, size and stability of CCL NPs and R-mAb-CD326@CCL NPs were investigated by DLS and TEM. The *in vitro* drug release behavior of CCL NPs was also studied. The results showed that the CCL NPs exhibited reduction-responsiveness and were able to release the original drug CUR under 10 mM GSH conditions. Additionally, the CCL NPs exhibited excellent stability in both the simulated body fluid environment and organic solvents. Especially, R-mAb-CD326@CCL NPs can actively target tumor cells and showed better therapeutic efficacy in *in vivo* experiments with a tumor suppression rate of 78.7%. This work provides a new idea for the design of nano-drugs targeting breast cancer.

Received 28th July 2023,
Accepted 11th September 2023

DOI: 10.1039/d3tb01703f

rsc.li/materials-b

Introduction

According to the statistical study conducted by the American Cancer Society in 2023, the number of new cancer cases and

deaths is over one million each year.¹ And the high incidence and low survival rate of cancer have seriously endangered human health.² The current treatment methods mainly include surgery, chemotherapy and radiotherapy. Among them, most traditional chemotherapy drugs cannot accumulate high concentrations at the tumor sites and have significant toxic side effects.³ With the development of materials science and pharmacology, the use of nanotechnology to deliver anti-cancer drugs has highlighted its advantages and become a research hotspot.^{4–6} How to improve the stability of nanoparticles and achieve precise targeted drug delivery are two key issues in this field.^{7–10}

Currently, it is widely believed that micelles formed by amphiphilic polymers in solution can be used as drug carriers to encapsulate hydrophobic anti-cancer drugs in micelles for *in vivo* drug delivery to disease sites.¹¹ However, the nano-structures of self-assembled micelles often undergo dissociation

^a College of Chemistry, Chemical Engineering and Materials Science, State and Local Joint Engineering Laboratory for Novel Functional Polymeric Materials, Jiangsu Key Laboratory of Advanced Functional Polymer Design and Application, Suzhou Key Laboratory of Macromolecular Design and Precision Synthesis, Soochow University, Suzhou 215123, P. R. China. E-mail: phni@suda.edu.cn; Tel: +86-512-65882047

^b Institute of Functional Nano and Soft Materials (FUNSOM), Soochow University, Suzhou, 215123, P. R. China

^c Intervention Department, The Second Affiliated Hospital of Soochow University, Suzhou, Jiangsu 215123, P. R. China. E-mail: sdfeyxsw@163.com

† Electronic supplementary information (ESI) available: Specific synthesis steps, ¹H NMR of HO-ss-Br, HO-ss-N₃, FT-IR of APEG-*b*-PBYP, MALDI-TOF MS of R-mAb-CD326, images of tumors after treatments and molecular weights and dispersity (D) of APEG-*b*-PBYP. See DOI: <https://doi.org/10.1039/d3tb01703f>

under the conditions of dilution or high concentrations, resulting in drug leakage and early release in the body. To overcome this problem, researchers utilize covalent bond cross-linking at the cores, shells or interfaces of the micelles to prevent micellar dissociation and regulate drug release behavior.^{12–15} These systems can be designed as stimuli-responsive linkages so that the cross-linked bonds can be available for degradation or hydrolysis under specific conditions, such as low pH or reducing environments. In these cases, drugs are released almost exclusively in the cancerous tissue or cancer cells, enabling the minimization of drug leakage during blood circulation.^{16–19}

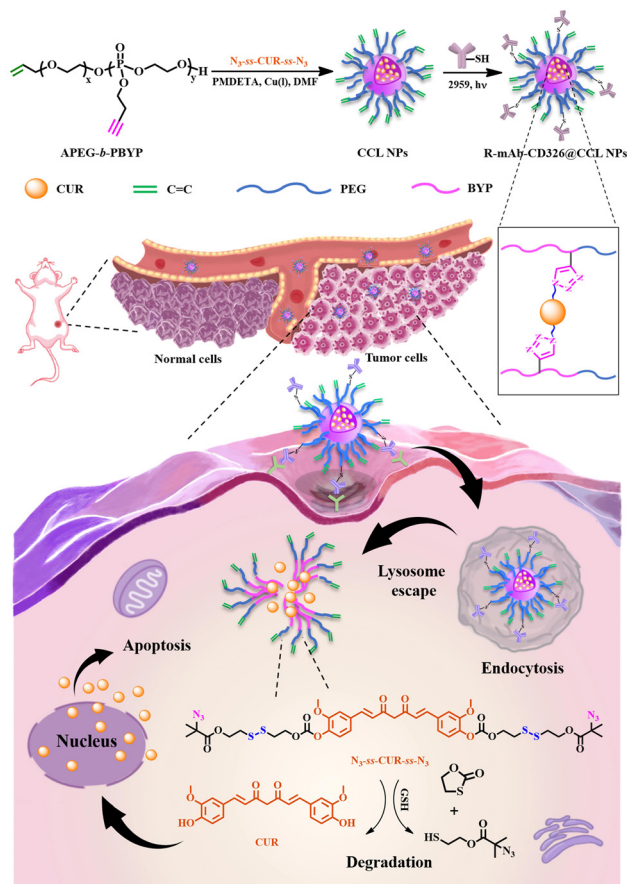
In recent reports, researchers proposed that the surface of nano-drugs can be modified by various specific target molecules, such as antibodies, aptamers, peptides, nucleic acids, affibodies and chemical small molecules, so that the drug delivery system can be recognized and internalized by cancer cells, and the precise release of drugs at tumor sites can be achieved.^{20–26} There are multiple highly expressed proteins at the tumor site, and the corresponding monoclonal antibodies can serve as targeting molecules for anti-cancer drugs due to their easy modification, strong specific recognition ability, and good biosafety.^{27,28}

The most common modification sites of antibodies are cysteine residues containing sulfhydryl groups (also called “thiol groups”) and lysine residues containing amino groups.^{29,30} Among them, the cysteine modification method has higher reactivity, but the number of free thiol groups in the antibody is very low. Therefore, when coupling antibodies to the surface of drug loaded nanoparticles, it is necessary to reduce the disulfide bonds of the antibody to produce more thiol groups.³¹ The commonly used type of antibody is IgG, an immunoglobulin composed of two heavy and two light chains covalently linked by disulfide bonds between chains. Disulfide bonds can be broken by reducing reagents such as dithiothreitol (DTT) and tris(2-chloroethyl) phosphate (TCEP), as they are easily exposed to solvents.³² By controlling the feed ratio of the reducing agent, the molecular weight of the reduced antibody fragment can be controlled, so that the product can still maintain the antigen binding sites.³³ CD326 monoclonal antibody (mAb-CD326) can specifically recognize the EpCAM (CD326) protein derived from epithelial tumors, which is highly expressed in epithelial tumors. Researches have shown that in various cancers (such as the colon, pancreas, bladder, prostate, breast, and ovary and hepatoblastoma), the positive rate of CD326 in tumor cells is higher than that in the corresponding normal tissues.^{34–36} Among them, breast cancer is a kind of tumor formed by uncontrolled proliferation of breast epithelial cells under the action of various carcinogenic factors. Therefore, mAb-CD326 can be used to target and identify breast cancer cells and induce an immune response to kill them.³⁷ At the same time, it does not cause damage to normal epithelium, because the boundary between cells is a very dense and highly organized structure.³⁸

It is worth noting that the disruption of inflammatory pathways plays a key role in cancer treatment.^{39,40} Inflammation induces an increase in pro-inflammatory cytokines and

transcription factors, leading to cancer cell proliferation and tumor growth, such as tumor necrosis factor- α (TNF- α), interleukins, nuclear factor- κ B (NF- κ B), and signal transducer and activator of transcription 3 (STAT3).⁴¹ TNF- α excitation activates NF- κ B, which further regulates cytokines such as interleukin (IL)-1, IL-2 and interferon gamma (IFN- γ). STAT3 is described as a common target of several signaling pathways that regulate oncogenes, pro-inflammatory cytokines, and growth factor transduction. This factor contributes to cell growth and survival by increasing the expression of anti-apoptotic proteins such as Bcl-2 and Bcl-xL. Curcumin (CUR) is a small molecule hydrophobic drug that can exert anti-inflammatory and anti-cancer functions by modulating several immune pathways, such as NF- κ B, STAT3, and TNF- α , and thus has anti-cancer properties against a variety of cancers, including lung, breast and prostate cancers.^{42,43} Meanwhile, CUR is a naturally derived small molecule anti-cancer drug with low cytotoxicity, low price, and abundant sources. Its polyphenolic structure has chemical activity and is easy to modify.^{44,45} It can be converted into a cross-linking agent through various chemical reactions. When nanomedicine enters the tumor environment, stimuli response of the connecting group causes the sensitive bonds to break and release the original drug.

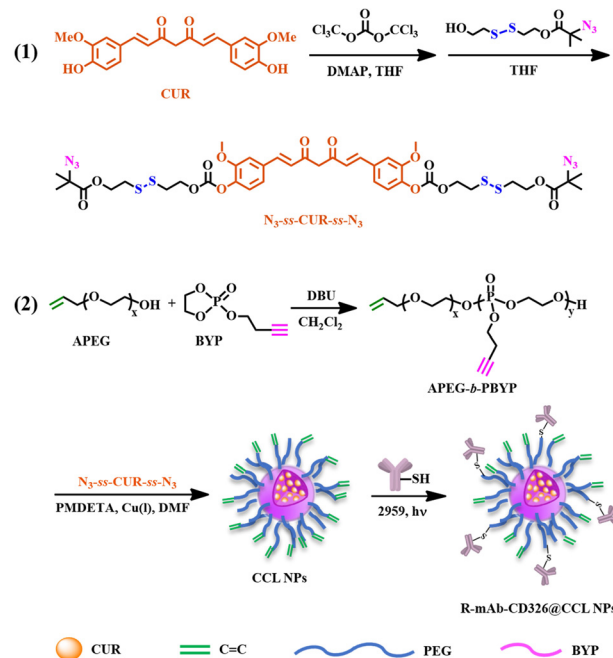
We have previously reported that core cross-linked polymer micelles are crosslinked with polyphosphoester containing azide groups at both ends as a crosslinking agent, or with lipoic acid groups of polymer side groups.^{46–49} As a new attempt, herein, we design a curcumin derivative containing double azide groups (N_3 -ss-CUR-ss- N_3) as crosslinking agents and modify mAb-CD326 on the surface of the nanoparticles. The resulting polymer nanoparticles have the following advantages: (i) increasing the drug loading of the nanoparticles, (ii) maintaining the stability of the nanoparticles in the physiological environment, and (iii) breaking the disulfide bond connecting CUR in the tumor cell microenvironment, releasing the original drug. As shown in Scheme 1, we first synthesized a CUR derivative as the hydrophobic core crosslinker N_3 -ss-CUR-ss- N_3 by modifying the hydroxyl group of CUR. Redox-sensitive disulfide bonds were introduced into the derivative, which will be broken to release the original CUR in response to the high concentration of glutathione (GSH) stimulation at the tumor sites. Then, the hydrophobic polymer APEG-*b*-PBYP was prepared by ring-opening polymerization of 2-(but-3-yn-1-yloxy)-2-oxo-1,3,2-dioxaphospholane (BYP) with APEG-OH. It was bonded by N_3 -ss-CUR-ss- N_3 to obtain the nano prodrugs (abbreviated as APEG-*b*-PBYP-ss-CUR), which can be dispersed in aqueous solution to form the core cross-linked nanoparticles (CCL NPs). In the next step, mAb-CD326 was reduced and conjugated at the end of the hydrophilic PEG chain through the Michael addition reaction to obtain drug loaded nanoparticles with surface modified mAb-CD326 (R-mAb-CD326@CCL NPs). When the drug is injected into mice, the nanoparticles can actively target and recognize highly expressed protein receptors on the surface of tumor cells, thus delivering the drug to the tumor sites and achieving specific release of CUR due to the special tumor microenvironment.



Scheme 1 Schematic diagram of the preparation of R-mAb-CD326@CCL NPs and their endocytosis by tumor cells and triggering CUR release in the cancer cytoreductive environment.

Results and discussion

Firstly, we synthesized a curcumin derivative (N_3 -ss-CUR-ss- N_3) as the hydrophobic core crosslinker. As shown in Scheme 2, the phenolic hydroxyl groups of CUR were activated with triphosgene and reacted with 2'-azidoisobutyryloxy-2-hydroxyethyl disulfide (OH-ss- N_3) to obtain N_3 -ss-CUR-ss- N_3 . Subsequently, using the hydroxyl group of allyl polyethylene glycol (APEG-OH) as an initiator, an amphiphilic diblock copolymer (APEG-*b*-PBYP) was prepared through ring opening polymerization of the BYP monomer, in which the alkynyl groups in the side groups of the PBYP chain could react with the azide groups of N_3 -ss-CUR-ss- N_3 via a copper-catalyzed Huisgen azide-alkyne cycloaddition reaction (CuAAC click chemistry) to obtain the prodrug APEG-*b*-PBYP-ss-CUR, followed by dispersion in aqueous solution to form core cross-linked nanoparticles (CCL NPs). In another reaction, the disulfide bonds between the chains of mAb-CD326 were reduced to yield thiol groups by the reducing agent TCEP. Finally, the surface of cross-linked prodrug nanoparticles (CCL NPs) was modified by the reduced mAb-CD326 to form R-mAb-CD326@CCL NPs through the "click" reaction between the allyl group at the end of PEG and the mercaptan group of R-mAb-CD326.



Scheme 2 Synthetic routes to core cross-linked nanoparticles modified by the CD326 monoclonal antibody (R-mAb-CD326@CCL NPs).

Characterization of N_3 -ss-CUR-ss- N_3 , APEG-*b*-PBYP and APEG-*b*-PBYP-ss-CUR

The reduction-responsive core cross-linker N_3 -ss-CUR-ss- N_3 was synthesized in three steps, and the products of each reaction step were characterized by ¹H NMR. Fig. S1 and S2 in the ESI,[†] show the ¹H NMR spectra of HO-ss-Br and HO-ss- N_3 . Fig. 1(a) shows the ¹H NMR spectrum of N_3 -ss-CUR-ss- N_3 . It can be seen that all chemical shifts correspond to the protons in N_3 -ss-CUR-ss- N_3 . Moreover, compared with the ¹H NMR spectrum of the intermediate HO-ss- N_3 , peak 6 to peak 12 in Fig. 1(a) represent the proton signals of CUR. To further demonstrate the

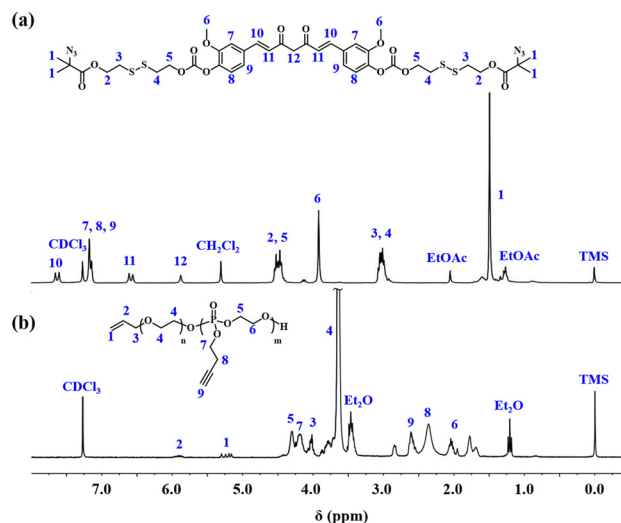


Fig. 1 ¹H NMR spectra of (a) N_3 -ss-CUR-ss- N_3 and (b) APEG-*b*-PBYP (solvent: CDCl₃).

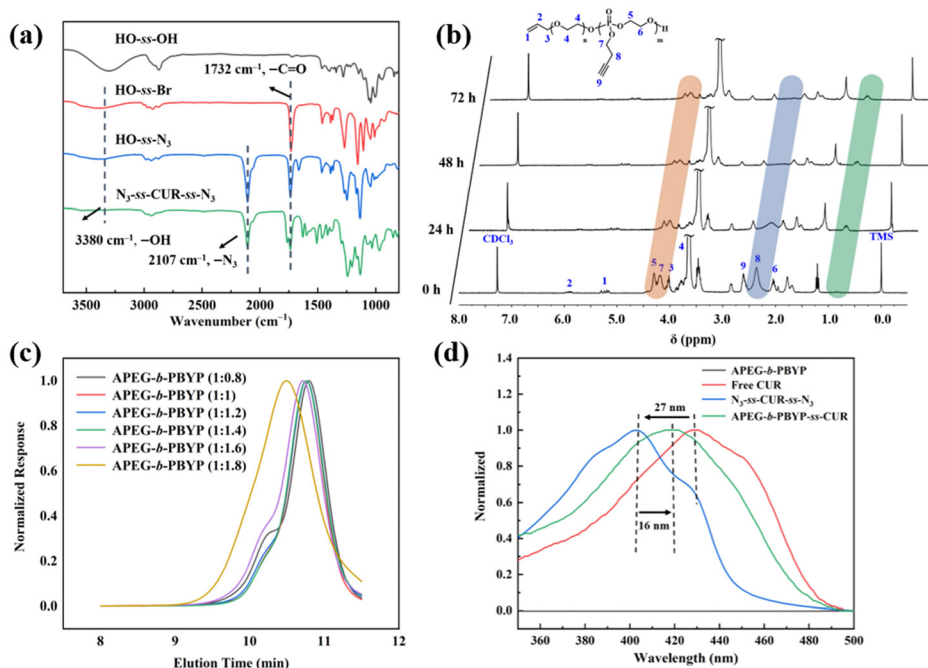


Fig. 2 Structural characterization: (a) FT-IR spectra of HO-ss-OH, HO-ss-Br, HO-ss-N₃ and N₃-ss-CUR-ss-N₃; (b) ¹H NMR spectra of APEG-*b*-PBYP and its degradation products at incubation times of 24, 48, and 72 h respectively (solvent: CDCl₃). (c) GPC traces of APEG-*b*-PBYP with different feed ratios of hydrophilic and hydrophobic units. (d) UV-Vis spectra of APEG-*b*-PBYP, free CUR, N₃-ss-CUR-ss-N₃ and cross-linked prodrug APEG-*b*-PBYP-ss-CUR, respectively.

successful synthesis of N₃-ss-CUR-ss-N₃, the products of each reaction step were tested by FT-IR. As shown in Fig. 2(a), the disappearance of the hydroxyl peak and the appearance of the azide peak indicate that the bisphenol groups of CUR have been successfully modified to azide groups.

The hydrophobic BYP monomer was synthesized according to previous literature.^{50,51} To verify the successful preparation of the diblock copolymer APEG-*b*-PBYP, we used ¹H NMR, FT-IR and GPC to analyze the structure and molecular weight. Fig. 1(b) shows the ¹H NMR spectrum of APEG-*b*-PBYP. Each signal peak can be attributed to the corresponding proton in the APEG-*b*-PBYP structure. The FT-IR spectrum also displays the structural information in Fig. S3 in the ESI,[†] and a clear alkynyl peak appeared at 3270 cm⁻¹, indicating that the APEG-*b*-PBYP copolymer has been successfully prepared. In this work, a series of amphiphilic copolymers with different molecular weights of PBYP were prepared according to different feed ratios of hydrophilic and hydrophobic segments. The molecular weight and dispersity of the amphiphilic polymer APEG-*b*-PBYP were characterized by GPC. As shown in Fig. 2(c), the molecular weight of the polymers showed an overall increasing trend with the increase of the hydrophobic section (BYP), which indicates the successful preparation of amphiphilic copolymers. The specific data are listed in Table S1 in the ESI.[†] Considering the water solubility and the number of cross-linking sites, a copolymer APEG-*b*-PBYP with a ratio of hydrophilic to hydrophobic blocks of 1:1.2 was chosen for subsequent experiments.

As a drug carrier, it is necessary to consider the biodegradability of copolymers. The amphiphilic copolymer APEG-*b*-

PBYP contains polyphosphoester chains that can be decomposed by phosphodiesterase I (PDE I).^{52,53} Herein, ¹H NMR is used to monitor the degradation products of APEG-*b*-PBYP at different times in the presence of phosphodiesterase I (PDE I). As shown in Fig. 2(b), after incubation of APEG-*b*-PBYP in PB 7.4 solution of 0.5 mg mL⁻¹ of PDE I, the proton peaks at δ 2.3–2.4 ppm attributed to polyphosphoester gradually weakened from 0 h to 72 h until they disappeared. At the same time, a new chemical shift peak appeared at δ 0.85 ppm, indicating that the polyphosphoester in APEG-*b*-PBYP can undergo degradation reactions and has good biodegradability.

UV-Vis spectroscopy can be used to clearly characterize the absorption peak changes of original CUR, crosslinker and core cross-linked prodrugs. Fig. 2(d) shows the UV-Vis spectra of APEG-*b*-PBYP, free CUR, N₃-ss-CUR-ss-N₃ and cross-linked prodrug APEG-*b*-PBYP-ss-CUR, respectively. It can be seen that the maximum absorption peaks of free CUR and N₃-ss-CUR-ss-N₃ are at 429 nm and 403 nm, respectively. Compared with these two substances and the copolymer APEG-*b*-PBYP without UV absorption, the maximum UV absorption wavelength of the cross-linked polymer prodrug APEG-*b*-PBYP-ss-CUR has red-shifted to 419 nm. This proves that the alkynyl groups of the copolymer APEG-*b*-PBYP undergo an effective click reaction with the azide groups of the N₃-ss-CUR-ss-N₃ crosslinker.

Effect of different cross-linking degrees on drug loading

Three kinds of core cross-linked nano prodrugs were prepared by adjusting the feed ratios of N₃-ss-CUR-ss-N₃ and APEG-*b*-PBYP, and their drug contents were 8.3%, 10.8% and 14.4%,

Table 1 CUR contents of APEG-*b*-PBYP-ss-CUR with different cross-linking ratios

Samples	Feed ratio ($m_1:m_2$) ^a	Yield (%)	CUR contents (wt%)
APEG- <i>b</i> -PBYP-ss-CUR-1	10:7	62.5	8.3
APEG- <i>b</i> -PBYP-ss-CUR-2	10:8	69.8	10.9
APEG- <i>b</i> -PBYP-ss-CUR-3	10:9	61.8	14.4

^a $m_1:m_2$ is the mass ratio of APEG-*b*-PBYP and N₃-ss-CUR-ss-N₃.

respectively. The specific information is shown in Table 1. The results show an increase in drug loading as the degree of cross-linking rises. Considering that polymer prodrugs used for cellular and *in vivo* experiments should have high drug loading and good dispersity, we chose the sample APEG-*b*-PBYP-ss-CUR-2 in Table 1 for subsequent experiments.

Characterization of R-mAb-CD326

In this study, we used mouse mAb-CD326 (40 kDa) as the target molecule, which belongs to the immunoprotein IgG2a type. Its hinge region contains four pairs of interchain disulfide bonds, and they are easily reduced to fragments with thiol groups. The molecular weight of the reduced monoclonal antibodies (R-mAb-CD326) was characterized by MALDI-TOF MS. From Fig. S4 in the ESI,[†] it can be seen that the R-mAb-CD326 mainly exhibits peak signals at a mass/charge ratio of 23234. From the molecular weight, it can be inferred that the four pairs of disulfide bonds contained in the hinge region were basically reduced to thiol groups (–SH). Table 2 lists the thiol content of the antibodies before and after reduction, which were determined using the DTNB sulfhydryl assay kit as 0.59 and 7.6 (molar ratio), respectively. Afterwards, different antibody feed ratios were set and the grafting rate of the reduced monoclonal antibody (R-mAb-CD326) on the surface of CCL NPs was measured using a BCA kit. As shown in Table 2, after reduction, the grafting rate of R-mAb-CD326 has significantly increased. In the control groups with different mass ratios of mAb-CD326 to CCL NPs, the reduced antibody had the highest grafting rate when the feeding ratio of mAb-CD326 and CCL NPs was 1:1000. Considering the balance between cost and antibody grafting rate, we chose the sample named R-mAb-CD326@CCL NPs-2 in Table 2 for subsequent experiments, and uniformly referred to as R-mAb-CD326@CCL NPs.

Morphology and size analysis of nanoparticles

Using transmission electron microscopy (TEM) and dynamic light scattering (DLS), we investigated the morphology and size of the antibody modified core cross-linked nanoparticles (R-mAb-CD326@CCL NPs) and the prodrug nanoparticles (CCL NPs) without antibody. As shown in Fig. 3(a) and (b), for the CCL NPs, the average particle size tested by DLS was 129 nm, while the particle size was around 100 nm measured by TEM. In contrast, the particle size of R-mAb-CD326@CCL NPs was 146 nm in Fig. 3(c), larger than that of CCL NPs. And the size measured by TEM was also around 110 nm, as shown in Fig. 3(d). These results indicate that the size of nanoparticles

Table 2 Sulfhydryl content of mAb-CD326 and ratios of mAb-CD326 grafted onto CCL NPs to the initial feed (grafting rate)

Samples	–SH content ($n_x:n_y$) ^a	Feeding ratio ($m_1:m_2$) ^b	Grafting rate (%)
mAb-CD326@CCL NPs	0.59	1:1000	19.1
R-mAb-CD326@CCL NPs-1	7.6	1:500	49.9
R-mAb-CD326@CCL NPs-2	7.6	1:1000	81.9
R-mAb-CD326@CCL NPs-3	7.6	1:2000	76.3

^a $n_x:n_y$ is the molar ratio of –SH and mAb-CD326. ^b $m_1:m_2$ is the mass ratio of mAb-CD326 and CCL NPs.

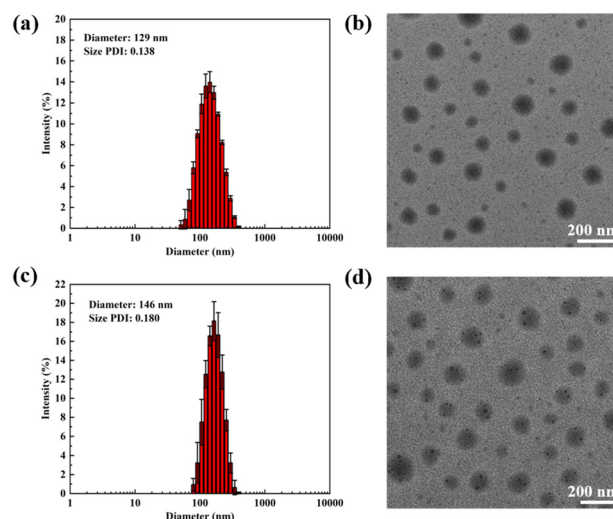


Fig. 3 Size distribution and morphology of nanoparticles: (a) histogram of particle size distribution and (b) TEM image of CCL NPs in PB 7.4 solution (concentration: 0.5 mg mL^{−1}). (c) Histogram of particle size distribution and (d) TEM image of R-mAb-CD326@CCL NPs in PB 7.4 solution (concentration: 0.5 mg mL^{−1}).

before and after coupling antibodies is appropriate and uniformly distributed for anticancer nano-drugs. The average particle size tested by DLS is slightly larger than that determined by TEM, because the hydrophilic chain of nanoparticles could collapse after freeze-drying when preparing the TEM samples, while the nanoparticles tested by DLS exist in aqueous solution with more spreading hydrophilic chains.

Stability of CCL NPs

The core cross-linked prodrug nanoparticles (CCL NPs) were prepared using crosslinker N₃-ss-CUR-ss-N₃ with stimulus responsiveness. Due to the existence of disulfide bonds, free CUR can be released in a reducing environment in the presence of glutathione (GSH). At the same time, CCL NPs should remain stable in a normal physiological environment. Herein, the particle size stability of prodrug nanoparticles under different conditions was tested by changing the concentration and medium. From Fig. 4(a), it can be seen that CCL NPs can remain stable in PB 7.4 solution for a long time. Since the core cross-linked bonds are disulfide bonds that can be cleaved by GSH, the nanoparticles tended to dissociate in the presence of

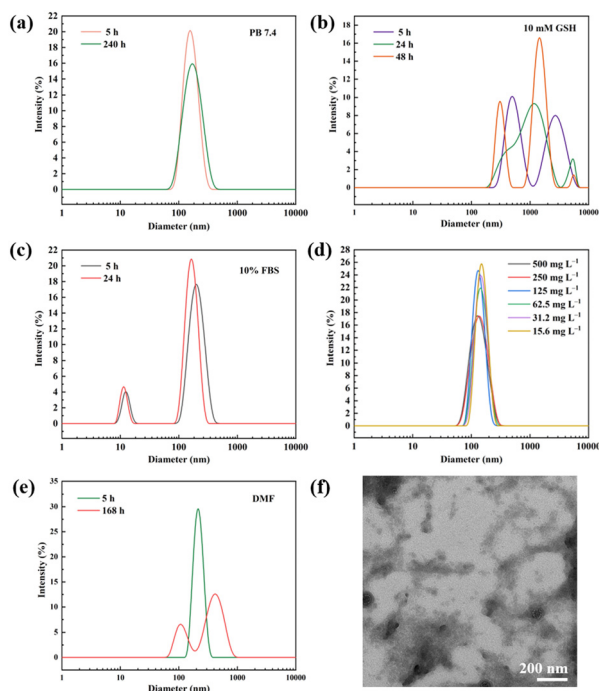


Fig. 4 Size distribution curves of nanoparticles under different conditions: (a) in PB 7.4 solution, (b) in PB 7.4 solution with 10 mM GSH, (c) in PB 7.4 solution with 10% FBS, (d) in PB 7.4 solution with different concentrations of CCL NPs, and (e) in DMF, and (f) TEM image of CCL NPs in PB 7.4 solution with 10 mM GSH after stirring for 48 h.

10 mM GSH as shown in Fig. 4(b), and large aggregated fragments of particles appeared. Fig. 4(f) shows the TEM image of CCL NPs in PB 7.4 solution containing 10 mM GSH after incubation for 48 h, and the phenomenon was consistent with the results shown in Fig. 4(b). In addition, the change curves of their particle size in PB 7.4 solution with 10% FBS were tested to study the stability of nanoparticles in blood circulation. The result shown in Fig. 4(c) indicates that the nanoparticles remained stable for 24 h, the peak at 10 nm belonged to the small nanoparticle aggregates contained in the serum itself. Fig. 4(d) shows the particle size distribution curves of different concentrations of CCL NPs in the aqueous phase, and the nanoparticles remained well distributed even in a very dilute concentration of 15.6 mg L⁻¹. Fig. 4(e) further demonstrates the storage stability of CCL NPs, which can maintain the micellar structure even in DMF. Overall, these experimental results confirmed the storage stability and good stimuli responsiveness of CCL NPs.

In vitro drug release

After demonstrating the good stability of CCL NPs, the *in vitro* drug release behavior was further investigated. Fig. 5(a) shows the CUR release curves of CCL NPs in PB 7.4 and PB 7.4 plus 10 mM GSH, respectively. It shows that CCL NPs could remain basically stable in the PB 7.4 solution, and the cumulative drug leakage of CUR was only about 10% at 144 h. However, in PB 7.4 plus 10 mM GSH, CUR drug release reached 60% at 72 h. As time passed, the drug continued to be released, and the

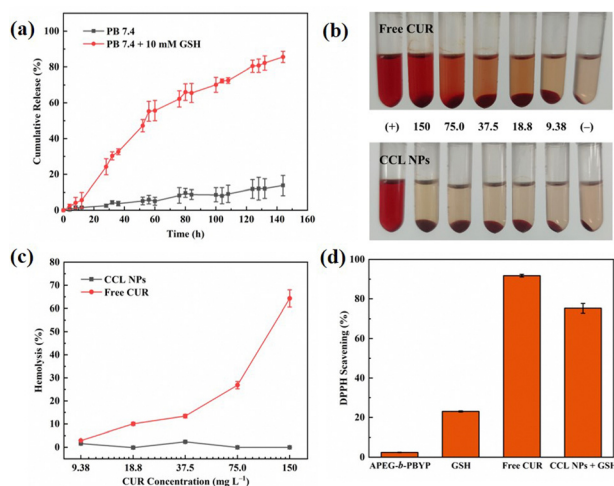


Fig. 5 (a) *In vitro* release of CUR from CCL NPs in different media, (b) photographs of free CUR and CCL NPs after incubation with erythrocytes for 4 h and (c) percentage of hemolysis. (d) DPPH scavenging percentage of APEG-*b*-PBYP, GSH, free CUR and CCL NPs with GSH, respectively.

cumulative drug release reached over 80% in 144 h. This indicates that in the tumor microenvironment, high GSH concentration can reduce and break the disulfide bonds linked to CUR, and the cross-linking structure in the prodrug nanoparticles is destroyed, making the nanoparticles tend to dissociate, thus releasing hydrophobic drug CUR. This is consistent with our previous research results shown in Fig. 4(b). In Scheme 1, the dissociation mechanism of crosslinker N₃-ss-CUR-ss-N₃ and the process of releasing CUR are presented.

In vitro hemolysis activity

When the prodrug is injected into the body, it will enter the bloodstream, so the prepared prodrug must have good blood compatibility. Fig. 5(b) is a photo of two sets of blood compatibility tests. It can be intuitively seen that compared with the control group, the CCL NPs group showed no significant hemolysis, and most red blood cells were concentrated at the bottom of the centrifuge tubes. A UV-Vis spectrophotometer was used to test the degree of ring-breaking of erythrocytes after incubation with free CUR and CCL NPs. As shown in Fig. 5(c), even at high CUR concentrations of 150 mg L⁻¹, the hemolysis rate of CCL NPs remained around 0%, while the free CUR group showed high hemolysis at the same high concentration of CUR, indicating that the prepared CCL NPs greatly improved the hemocompatibility of CUR.

In vitro DPPH radical scavenging

Free radicals increase dramatically during tumor formation and growth, and they may cause irreversible damage to the DNA of cells due to their strong oxidative properties.⁵⁴ The diketone and phenolic hydroxyl groups in the molecular structure of CUR can provide protons to block free radical reactions, so they can scavenge free radicals.⁵⁵ A free radical scavenging experiment was performed *in vitro* using the DPPH method (namely 1,1-diphenyl-2-trinitrophenylhydrazine). As shown in

Fig. 5(d), the copolymer APEG-*b*-PBYP had almost no ability to scavenge free radicals, while GSH can eliminate free radicals due to the presence of free thiol groups, but its efficiency is much lower than that of free CUR and CCL NPs that release free drugs under GSH conditions. The latter can achieve 91% and 75% free radical clearance within 30 min, respectively. This further proves that CCL NPs can responsively release free CUR in the presence of GSH and exert their ability to scavenge free radicals.

In vitro cytotoxicity and apoptosis

The CD326 expression levels on the surface of human umbilical vein endothelial cells (HUVEC cells) and breast cancer cells (MCF-7 cells) were determined by flow cytometry and PE-anti-human-CD326 flow antibody. Fig. 6(a) and (b) show that HUVEC cells basically did not express CD326, while MCF-7 highly expressed CD326, which was consistent with the previous research.³⁴ Therefore, the cytotoxicity, endocytosis and apoptosis-inducing ability of R-mAb-CD326@CCL NPs were investigated in cellular and animal experiments using MCF-7 cells as the high CD326-expressing cells and HUVEC cells as the low CD326-expressing cells.

For polymeric nano-drugs, the loaded drug should be responsively released within the tumor microenvironment to kill cancer cells, while the nanocarriers should be non-toxic to

normal and cancer cells. The biocompatibility of the polymeric nanocarrier APEG-*b*-PBYP on HUVEC cells and MCF-7 cells was evaluated by MTT assay. Fig. 6(c) shows the cell viability of APEG-*b*-PBYP after incubation with the two kinds of cells for 48 h. Even if the concentration of APEG-*b*-PBYP increased from 6.25 mg L⁻¹ to 200 mg mL⁻¹, the viability of the above two types of cells remained above 90%, indicating that the polymer carrier APEG-*b*-PBYP has good biocompatibility.

We also investigated the toxicity of CUR, CCL NPs and R-mAb-CD326@CCL NPs to MCF-7 cells using the MTT assay. From the cytotoxicity results shown in Fig. 6(d), we can find that the cell viability of all three groups of samples decreased with the increase of CUR concentration after incubation with MCF-7 cells for 48 h. This indicates that the toxicity of all three samples to MCF-7 cells is dose-dependent. As shown in Table 3, the half-inhibitory concentration (IC₅₀) values of CUR, CCL NPs and R-mAb-CD326@CCL NPs to MCF-7 cells were 1.07 mg L⁻¹, 3.34 mg L⁻¹, and 1.22 mg L⁻¹, respectively. Compared to free CUR, the toxicity of both CCL NPs and R-mAb-CD326@CCL NPs decreased, which was due to the reduction of nanoparticle biotoxicity by using a kind of biocompatible carrier, while R-mAb-CD326@CCL NPs exhibited higher cytotoxicity than CCL NPs. This may be due to the fact that nanoparticles modified by R-mAb-CD326 can better target tumor cells and enhance endocytosis.

To investigate the ability of R-mAb-CD326@CCL NPs to induce apoptosis of MCF-7 cells, we used the AnnexinV-APC/7-AAD cell apoptosis detection kit to detect the apoptosis of MCF-7 cells and compared R-mAb-CD326@CCL NPs with PBS, free CUR, and CCL NPs, respectively. In all tests, the incubation time was 48 h. As shown in Fig. 6(e), when the CUR dose was 6.25 mg L⁻¹, the apoptosis rate of MCF-7 cells in the R-mAb-CD326@CCL NP group was 42.9%, which was equivalent to the free CUR (41.4%), and much higher than CCL NPs (6.7%). And the late apoptosis rate of MCF-7 cells in the R-mAb-CD326@CCL NP group was 32.5%, which was higher than that of early apoptotic cells (10.4%).

Cellular uptake

CLSM was used to further evaluate the endocytosis behavior of free CUR, CCL NPs and R-mAb-CD326@CCL NPs. As shown in Fig. 7(a), with the extension of time, the nanoparticles were taken up by the cells. The green fluorescence of CUR appeared and the fluorescence increased with time. However, compared with the passive uptake behavior of CCL NPs without monoclonal antibodies, R-mAb-CD326@CCL NPs were able to actively identify cancer cells, so the green fluorescence emitted was significantly stronger, and some cyan fluorescence displayed by

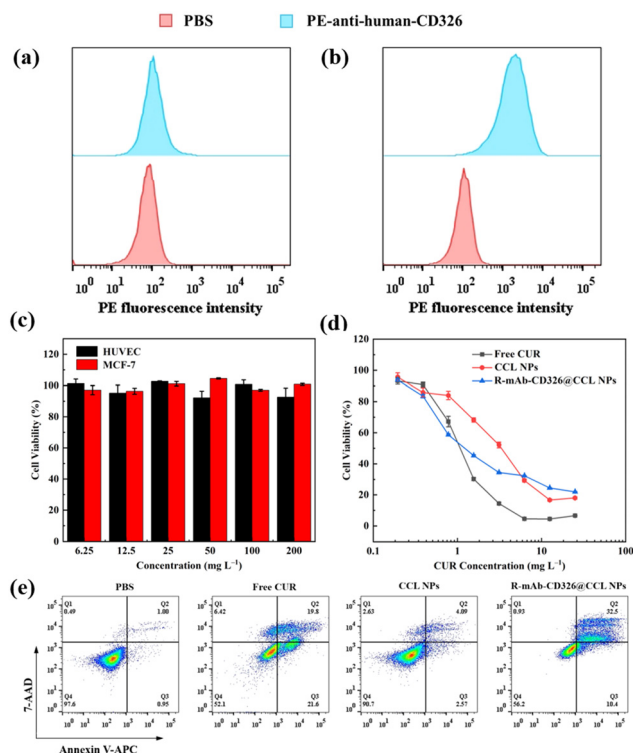


Fig. 6 The expression level of the CD326 protein on the surface of (a) HUVEC cells and (b) MCF-7 cells. (c) Cell viability of HUVEC cells and MCF-7 cells after incubation with APEG-*b*-PBYP at different concentrations for 48 h. (d) Cell viability and (e) apoptosis of MCF-7 cells incubated for 48 h with different doses of free CUR, CCL NPs and R-mAb-CD326@CCL NPs, respectively.

Table 3 IC₅₀ values of free CUR, CCL NPs and R-mAb-CD326@CCL NPs against MCF-7 cells

Samples	IC ₅₀ (mg L ⁻¹)
Free CUR	1.07
CCL NPs	3.34
R-mAb-CD326@CCL NPs	1.22

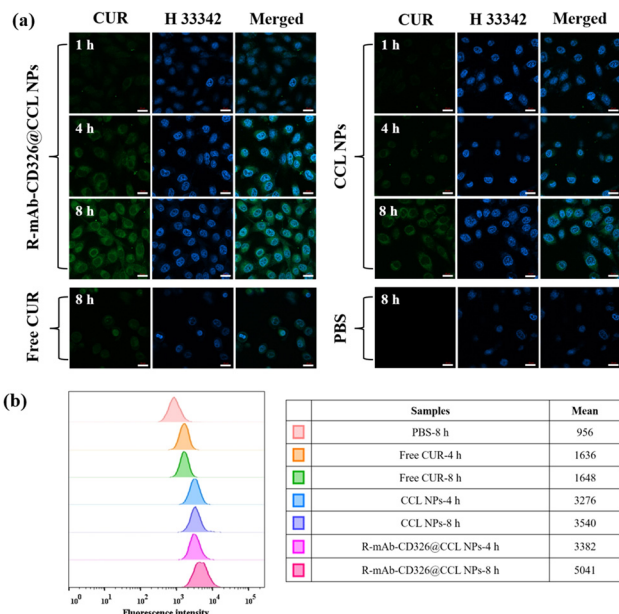


Fig. 7 (a) Intracellular fluorescence images, (b) flow cytometry curves of MCF-7 cells incubated with R-mAb-CD326@CCL NPs, CCL NPs, free CUR and PBS, respectively, for different times (scale bar: 20 μ m).

the overlap of the green fluorescence and the blue fluorescence can be clearly observed at 8 h, indicating that some drugs have successfully escaped from the lysosomes and entered into the cellular nucleus. In addition, the fluorescence in the free CUR group was very weak because the small molecule drug CUR was mainly endocytosed and exocytosed by the difference in intracellular and extracellular concentrations, which was difficult to trap and enrich in the tumor sites. Similarly, flow cytometry was used to quantify the drug fluorescence taken up by the cells. The same results as those measured by CLSM can be obtained from Fig. 7(b). The above statistics demonstrate that the core cross-linked nanoparticles can actively target and get better enrichment in MCF-7 cells after modification with the reduced monoclonal antibody R-mAb-CD326.

In vivo anti-tumor experiment

Animals were housed according to AAALAC (Association for Assessment and Accreditation of Laboratory Animal Care) guidelines. All animal-related experiments were conducted in full accordance with institutional guidelines, and were approved by the Advisory Committee on Animal Use and Care Management of the Second Affiliated Hospital of Soochow University. Laboratory animal practitioner number: 220228492.

The anti-tumor effect of R-mAb-CD326@CCL NPs in mice was studied using *in situ* breast cancer cell line. On the 10th day, after MCF-7 cells were inoculated, the tumor size of the mice was about 100 mm³. The dose of CUR was kept of 20 mg kg⁻¹ and given every 2 days for a total of 7 injections, and the mice were executed on the 14th day.

In vivo biodistribution and fluorescence imaging

To validate the targeting ability of R-mAb-CD326@CCL NPs in mice, tumors and organs (heart, liver, spleen, lungs, and

kidneys) of mice were removed to test their drug contents after treatment, and fluorescence images were recorded. As shown in Fig. 8(a), it can be intuitively seen that there was almost no drug fluorescence in normal tissues. In the CCL NPs group, weak fluorescence appeared in the tumor, while in the R-mAb-CD326@CCL NPs group, the fluorescence intensity of the tumor was very strong. In addition, Fig. 8(b) shows that the drug accumulation in organs was at a low level of less than 3% in all groups, and the CCL NPs group could accumulate at higher levels in the tumor due to the EPR effect. Most notably, the group of R-mAb-CD326@CCL NPs showed the highest drug distribution, reaching 8.8%. This provides strong evidence that R-mAb-CD326@CCL NPs can actively target tumor cells. These results are consistent with the above analysis.

In vivo anti-tumor efficacy

Fig. 8(c) shows that the body weight of the mice in each group did not change significantly during the treatment. This shows that the toxicity and side effects of the drugs are relatively low. As can be seen in Fig. 8(d), MCF-7 cells in the PBS group grew

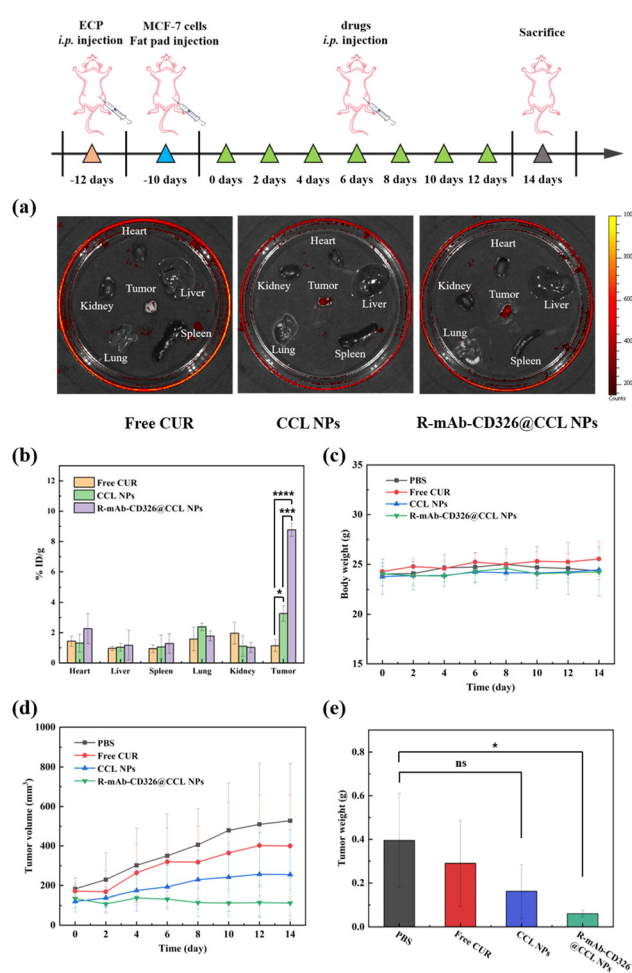


Fig. 8 Anti-tumor efficacy *in vivo*. (a) Fluorescence images and (b) drug distribution histograms of mice tumors and major organs on day 14. (c) Changes in mice body weight and (d) tumor volume during treatment. (e) Weight of tumor after treatment on day 14.

rapidly, reaching a mean tumor volume of 527 mm³ at the end of treatment. The free CUR group showed a less pronounced tumor suppressive effect and a mean volume of 400 mm³, while the CCL NPs group, which could be passively targeted to the tumor sites by the EPR effect, showed a stronger tumor suppression effect (254 mm³). In addition, the group of R-mAb-CD326@CCL NPs showed the best therapeutic effect (112 mm³) with 78.7% tumor suppression due to its ability to actively identify the highly expressed CD326 receptor on the tumor surface and increased the uptake of the drug by the cells. Meanwhile, a representative image of the tumors was taken after the mice were executed and are displayed in Fig. S5 in the ESI,[†] and the weight of the tumors was recorded as shown in Fig. 8(e) which was basically consistent with the volume measured before.

Histopathology and immunohistochemical analysis

H&E staining and immunohistochemistry (IHC) were further used to study the death of tumor cells in mice and their modulatory behavior towards cytokines after treatment with PBS, free CUR, CCL NPs and R-mAb-CD326@CCL NPs, respectively. As shown in Fig. 9, H&E staining of tumor tissue sections revealed the anti-tumor activity of R-mAb-CD326@CCL NPs. The tumor cells in the PBS group showed the best growth, the free CUR and CCL NPs groups showed different degrees of tumor cell necrosis. However, the tumor sections in the group of R-mAb-CD326@CCL NPs showed the largest area of necrosis with the number of tumor cells significantly reduced, accompanied by crumpling and rupture.

Immunohistochemistry (IHC) was used to analyze the expression of four types of cytokines (TNF- α , IFN- γ , Bcl-2 and NF- κ Bp65) in each group of tumors. Tumor necrosis factor TNF- α is one of the bioactive factors that can directly kill tumors. Interferon IFN- γ exerts anti-tumor effects by inhibiting

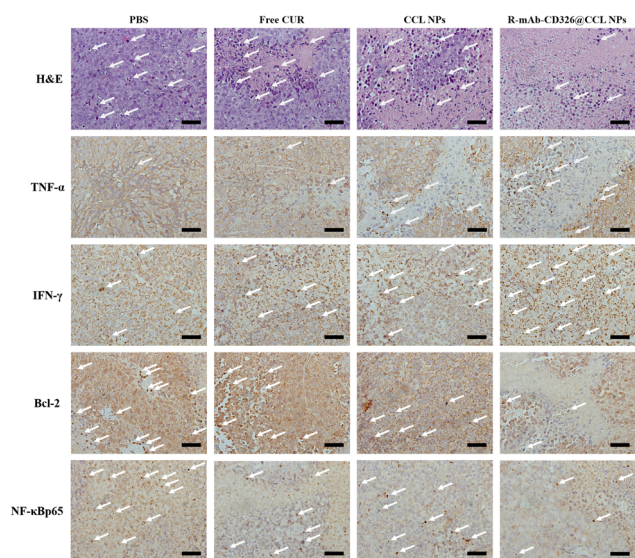


Fig. 9 H&E, immunohistochemistry (IHC) analyses of TNF- α , IFN- γ , Bcl-2 and NF- κ Bp65 expression (white arrows) of tumor slices on the 14th day of treatment (scale bar: 50 μ m).

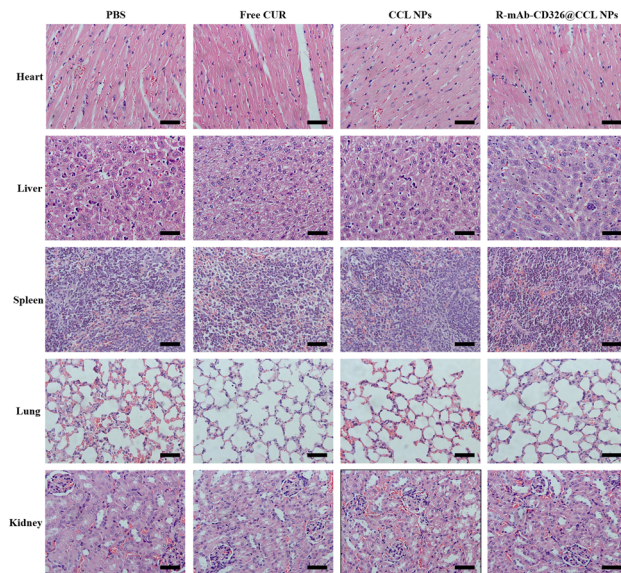


Fig. 10 H&E staining images of the heart, liver, spleen, lung and kidney sections of MCF-7 bearing mice treated with PBS, free CUR, CCL NPs and R-mAb-CD326@CCL NPs, respectively (scale bar: 50 μ m).

cell proliferation and modulating immunity. The anti-apoptotic gene Bcl-2 can inhibit the apoptosis of target cells induced by most chemotherapeutic drugs. The nuclear transcription factor NF- κ Bp65 can be activated and involved in inflammation and the development of many cancers. As shown in Fig. 9, a small amount of TNF- α and IFN- γ secretion was present in the PBS group due to the presence of some immune effect at the tumor sites. The distribution of TNF- α was less in necrotic tissues, but in the non-necrotic areas of the sections in the treatment groups, the expression of both TNF- α and IFN- γ were increased. For the tumor-promoting factors Bcl-2 and NF- κ Bp65, the PBS group showed abundant expression, while the treatment groups showed varying degrees of decreased expression. In the IHC results of each group, R-mAb-CD326@CCL NPs exhibited the best modulation effect. This suggests that R-mAb-CD326@CCL NPs can induce apoptosis in breast cancer tumor cells by regulating various signalling pathways.

The major organs of the mice were collected at the end of the treatment for H&E staining analysis (Fig. 10). Under the microscope, we could not observe significant damage on the slice of the heart, liver, spleen, lungs and kidneys in each group of mice, indicating that R-mAb-CD326@CCL NPs have good biocompatibility.

Conclusions

In this study, we design a kind of nanoparticles core cross-linked by a derivative of the natural small molecule drug curcumin (CUR), and modify the surface of the nanoparticles with the CD326 monoclonal antibody for active targeting of breast cancer tumors. The particle size of R-mAb-CD326@CCL NPs was 146 nm and uniform, which allows them to accumulate at the tumor site, and the drug can be continuously

released in a reducing environment. In cellular assays, R-mAb-CD326@CCL NPs showed good inhibitory and apoptosis effects on MCF-7 cells. *In vivo* experiments also demonstrated that R-mAb-CD326@CCL NPs were able to actively target tumor sites and greatly enhance the bioavailability of CUR. Furthermore, R-mAb-CD326@CCL NPs had good therapeutic effect with a tumor inhibition rate of 78.7%. This work provides a new idea for improving the smart responsiveness of drugs and the structural design of targeted nano-drugs. The strategy using the drug derivative as the core crosslinker for micelles avoided the possible risks associated with the introduction of off-system crosslinkers, greatly improved the stability of nanoparticles, reduced drug leakage in normal tissues, and responsively released the drug under the reducing conditions of the tumor microenvironment. Meanwhile, the carriers are biodegradable, which can be decomposed by enzymes and metabolized by the human body. The above characteristics of R-mAb-CD326@CCL NPs make them a kind of promising new targeted nano-drug for breast cancer treatment.

Conflicts of interest

There are no conflicts to declare.

Acknowledgements

This research was supported by the National Natural Science Foundation of China, grant number 21975169; the Project Fund of the Priority Academic Program Development (PAPD) of Jiangsu Higher Education Institutions; the Key Laboratory of Polymeric Materials Design and Synthesis for Biomedical Function of Soochow University; and the Young Talent Program of China National Nuclear Corporation, grant number CNNC51007.

Notes and references

- R. L. Siegel, K. D. Miller, N. S. Wagle and A. Jemal, *CA Cancer J. Clin.*, 2023, **73**, 17–48.
- F. Bray, J. Ferlay, I. Soerjomataram, R. L. Siegel, L. A. Torre and A. Jemal, *CA Cancer J. Clin.*, 2018, **68**, 394–424.
- S. Y. Qin, A. Q. Zhang and X. Z. Zhang, *Small*, 2018, **14**, 1802417.
- F. Abedi-Gaballu, G. Dehghan, M. Ghaffari, R. Yekta, S. Abbaspour-Ravasjani, B. Baradaran, J. E. N. Dolatabadi and M. R. Hamblin, *Appl. Mater. Today*, 2018, **12**, 177–190.
- J. Jampilek and K. Kralova, *Materials*, 2021, **14**, 1059.
- W. T. Xia, Z. X. Tao, B. Zhu, W. X. Zhang, C. Liu, S. Y. Chen and M. M. Song, *Int. J. Mol. Sci.*, 2021, **22**, 9118.
- M. L. Goas, J. Saber, S. G. Bolívar, J. M. Rabanel, J. M. Awogni, D. C. Boffito and X. Banquy, *Nano Today*, 2022, **45**, 101516.
- M. X. Zhou, J. Y. Zhang, X. M. Cai, R. Dou, L. F. Ruan, W. J. Yang, W. C. Lin, J. Chen and Y. Hu, *Chin. J. Polym. Sci.*, 2023, **41**, 525–537.
- H. R. Tian, L. Yu, M. Z. Zhang, J. L. He, X. W. Sun and P. H. Ni, *Colloids Surf., B*, 2023, **228**, 113400.
- W. Y. Ban, Q. H. Luo, C. D. Yan, X. Y. Fan, G. R. Zhu, M. S. Cheng, Z. G. He, M. C. Sun and J. Sun, *Nano Res.*, 2023, **16**(5), 7422–7430.
- H. Cabral and K. Kataoka, *J. Controlled Release*, 2014, **190**, 465–476.
- B. J. Li, Y. Q. Wu, Y. Wang, M. S. Zhang, H. M. Chen, J. Li, R. H. Liu, Y. Ding and A. G. Hu, *ACS Appl. Mater. Interfaces*, 2019, **11**, 8896–8903.
- L. X. Zhang, D. W. Zhang, Y. F. Yang and Y. Zhang, *Langmuir*, 2021, **37**, 3950–3959.
- C. K. Chen, W. J. Lin, Y. Hsia and L. W. Lo, *Macromol. Biosci.*, 2017, **17**, 1600191.
- Y. Zhou, Y. W. Zhang, C. Q. Jiang, Y. X. Chen, F. Tong, X. T. Yang, Y. Z. Wang, X. Xia and H. L. Gao, *Small*, 2023, **19**, 2300594.
- W. X. Chen, Y. F. Cheng and B. H. Wang, *Angew. Chem., Int. Ed.*, 2012, **51**, 5293–5295.
- Y. P. Li, K. Xiao, W. Zhu, W. B. Deng and K. S. Lam, *Adv. Drug Delivery Rev.*, 2014, **66**, 58–73.
- R. J. Banga, B. Meckes, S. P. Narayan, A. J. Sprangers, S. T. Nguyen and C. A. Mirkin, *J. Am. Chem. Soc.*, 2017, **139**, 4278–4281.
- H. J. Qu, J. F. Yang, S. J. Li, J. Xu, X. Zhou, X. D. Xue, D. L. Zhang, H. X. Du, Y. B. Shen, M. Ramachandran, H. B. Zheng, Y. Wu, Y. F. Ding, H. Wu, X. B. Ma, T. Y. Lin and Y. P. Li, *J. Controlled Release*, 2023, **357**, 274–286.
- Y. M. Yang, Y. Han, Q. Y. Sun, J. Cheng, C. X. Yue, Y. L. Liu, J. Song, W. L. Jin, X. T. Ding, J. M. de la Fuente, J. Ni, X. Q. Wang and D. X. Cui, *J. Nanobiotechnol.*, 2021, **19**, 54.
- P. Q. Li, J. D. Han, D. Li, J. J. Chen, W. Wang and W. G. Xu, *Polymers*, 2018, **10**, 611.
- R. Zhou, M. Z. Zhang, J. L. He, J. Liu, X. W. Sun and P. H. Ni, *ACS Omega*, 2022, **7**, 21325–21336.
- X. Y. Yang, X. L. Xia, W. Huang, X. X. Xia and D. Y. Yan, *Nano Res.*, 2023, **16**(4), 5256–5264.
- L. Li, Y. Song, J. L. He, M. Z. Zhang, J. Liu and P. H. Ni, *J. Mater. Chem. B*, 2019, **7**, 786–795.
- J. Hu, X. W. Yuan, F. Wang, H. L. Gao, X. L. Liu and W. Zhang, *Chin. Chem. Lett.*, 2021, **32**, 1341–1347.
- J. X. He, Q. Duan, C. Y. Ran, T. Fu, Y. Liu and W. H. Tan, *Acta Pharm. Sin. B*, 2023, **13**(4), 1358–1370.
- Y. Zhou, L. Wang, L. F. Chen, W. Wu, Z. M. Yang, Y. Z. Wang, A. Q. Wang, S. J. Jiang, X. Z. Qin, Z. C. Ye, Z. Y. Hu and Z. H. Wang, *Nano Res.*, 2023, DOI: [10.1007/s12274-023-5921-6](https://doi.org/10.1007/s12274-023-5921-6).
- S. Y. Wu, F. G. Wu and X. Y. Chen, *Adv. Mater.*, 2022, **34**, 2109210.
- S. J. Walsh, J. D. Bargh, F. M. Dannheim, A. R. Hanby, H. Seki, A. J. Counsell, X. X. Ou, E. Fowler, N. Ashman, Y. Takada, A. Isidro-Llobet, J. S. Parker, J. S. Carroll and D. R. Spring, *Chem. Soc. Rev.*, 2021, **50**, 1305–1353.
- V. P. Chavda, P. C. Balar, D. Teli, M. Davidson, J. Bojarska and V. Apostolopoulos, *Molecules*, 2023, **28**, 2605.
- W. K. Chung, B. Russell, Y. H. Yang, M. Handlogten, S. Hudak, M. Y. Cao, J. H. Wang, D. Robbins, S. Ahuja and M. Zhu, *Biotechnol. Bioeng.*, 2017, **114**(6), 1264–1274.

- 32 H. Sharma and R. Mutharasan, *Anal. Chem.*, 2013, **85**, 2472–2477.
- 33 Y. L. Song, H. Cai, Z. J. Tan, N. Mussa and Z. J. Li, *Appl. Microbiol. Biotechnol.*, 2022, **106**, 1057–1066.
- 34 C. Patriarca, R. M. Macchi, A. K. Marschner and H. Mellstedt, *Cancer Treat. Rev.*, 2012, **38**, 68–75.
- 35 S. Armeanu-Ebinger, A. Hoh, J. Wenz and J. Fuchs, *OncolImmunology*, 2013, **2**(1), e22620.
- 36 O. Pershina, N. Ermakova, A. Pakhomova, D. Widera, E. Pan, M. Zhukova, E. Slonimskaya, S. G. Morozov, A. Kubatiev, A. Dygai and E. G. Skurikhin, *Biomedicines*, 2021, **9**, 1223.
- 37 J. Macdonald, J. Henri, K. Roy, E. Hays, M. Bauer, R. N. Veedu, N. Pouliot and S. Shigdar, *Cancers*, 2018, **10**, 19.
- 38 M. Amann, M. Friedrich, P. Lutterbuese, E. Vieser, G. Lorenczewski, L. Petersen, K. Brischwein, P. Kufer, R. Kischel, P. A. Baeuerle and B. Schlereth, *Cancer Immunol. Immun.*, 2009, **58**, 95–109.
- 39 Y. Z. Wu, S. Antony, J. L. Meitzler and J. H. Doroshov, *Cancer Lett.*, 2014, **345**, 164–173.
- 40 B. Z. Qian, *Semin. Cancer Biol.*, 2017, **47**, 170–176.
- 41 A. Giordano and G. Tommonaro, *Nutrients*, 2019, **11**, 2376.
- 42 V. Zoi, V. Galani, G. D. Lianos, S. Voulgaris, A. P. Kyritsis and G. A. Alexiou, *Biomedicines*, 2021, **9**, 1086.
- 43 M. Catanzaro, E. Corsini, M. Rosini, M. Racchi and C. Lanni, *Molecules*, 2018, **23**, 2778.
- 44 F. C. Rodrigues, N. V. A. Kumar and G. Thakur, *Eur. J. Med. Chem.*, 2019, **177**, 76–104.
- 45 M. A. Tomeh, R. Hadianamrei and X. B. Zhao, *Int. J. Mol. Sci.*, 2019, **20**, 1033.
- 46 J. Hu, J. L. He, M. Z. Zhang and P. H. Ni, *Polym. Chem.*, 2015, **6**, 1553–1566.
- 47 J. Hu, J. L. He, D. L. Cao, M. Z. Zhang and P. H. Ni, *Polym. Chem.*, 2015, **6**, 3205–3216.
- 48 Y. Sun, X. Q. Du, J. L. He, J. Hu, M. Z. Zhang and P. H. Ni, *J. Mater. Chem. B*, 2017, **5**, 3771–3782.
- 49 Y. W. Cao, J. L. He, J. Liu, M. Z. Zhang and P. H. Ni, *ACS Appl. Mater. Interfaces*, 2018, **10**, 7811–7820.
- 50 S. Y. Zhang, A. Li, J. Zou, L. Y. Lin and K. L. Wooley, *ACS Macro Lett.*, 2012, **1**, 328–333.
- 51 Y. H. Lim, G. S. Heo, S. Cho and K. L. Wooley, *ACS Macro Lett.*, 2013, **2**, 785–789.
- 52 F. W. Zhang, S. Y. Zhang, S. F. Pollack, R. Li, A. M. Gonzalez, J. W. Fan, J. Zou, S. E. Leininger, A. Pavia-Sanders, R. Johnson, L. D. Nelson, J. E. Raymond, M. Elsabahy, D. M. P. Hughes, M. W. Lenox, T. P. Gustafson and K. L. Wooley, *J. Am. Chem. Soc.*, 2015, **137**, 2056–2066.
- 53 T. Rheinberger, M. Deuker and F. R. Wurm, *Eur. Polym. J.*, 2023, **190**, 111999.
- 54 B. Akbari, N. Baghaei-Yazdi, M. Bahmaie and F. M. Abhari, *BioFactors*, 2022, **48**, 611–633.
- 55 H. T. Kevij, M. Salami, M. Mohammadian and M. Khodadadi, *Food Hydrocolloids*, 2020, **108**, 106026.